Inorganic Chemistry
Article
Cite This: Inorg. Chem. XXXX, XXX, XXX−XXX
pubs.acs.org/IC

The Fluorine Effect in Zwitterionic Half-Sandwich Iridium(III) Anticancer Complexes

Yanjing Yang, Lihua Guo,* Xingxing Ge, Teng Zhu, Wenjing Chen, Huanxing Zhou, Liping Zhao, and Zhe Liu*

Institute of Anticancer Agents Development and Theranostic Application, The Key Laboratory of Life-Organic Analysis and Key Laboratory of Pharmaceutical Intermediates and Analysis of Natural Medicine, Department of Chemistry and Chemical Engineering, Qufu Normal University, Qufu 273165, People's Republic of China

Supporting Information

ABSTRACT: The rational design by the introduction of fluorine into a compound has achieved success in the development of organic anticancer drugs. However, the fluorine effect in metal-based anticancer complexes has rarely been reported. In this contribution, we report the synthesis, characterization, chemical reactivity, and biological activity of a series of half-sandwich zwitterionic iridium(III) complexes containing different substituents in the η^5-Cp^R ring. The molecular structures for complexes **Ir1**−**Ir4** and **Ir7** were determined by single-crystal X-ray crystallography techniques. Notably, the asymmetrically substituted fluoro complexes **Ir4** and **Ir6** in solution show two conformational isomers. These complexes have sufficient stability, exhibit fluorescence emission, and show potent catalytic activity in converting NADH to NAD$^+$. The effect of the substituents in the η^5-Cp^R ring for these zwitterionic complexes on their anticancer activity was systematically investigated. Surprisingly, the presence of fluorinated substituents gives rise to a significant increase in the anticancer activity. The lipophilicity and cellular uptake levels of these complexes appeared to be the primary factors for their cytotoxicity in this system. A microscopic mechanism study showed that the typical complex **Ir4** entered A549 cancer cells through an energy-dependent pathway and was mainly located in lysosomes. Furthermore, an increase in ROS level, apoptosis induction, and cell-cycle perturbation together contribute to the anticancer potency of these zwitterionic complexes.

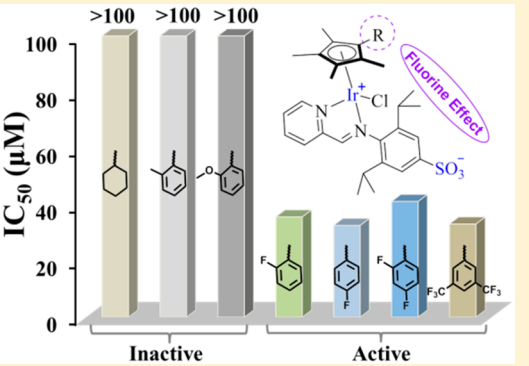

INTRODUCTION

The clinical success of cisplatin and its derivatives[1,2] has stimulated the exploration for other alternative metal-based anticancer drugs.[3−5] These novel metal-based anticancer drugs could address the limitations of platinum-based drugs such as toxic side effects and the progressive acquisition of drug resistance. Very recently, half-sandwich ruthenium(II) and iridium(III) anticancer complexes of the type (η^6-arene)Ru(XY)Cl and [(η^5-C_5Me_5)Ir(XY)Cl]$^{0/+}$, respectively, where XY is a bidentate chelating ligand, have attracted much attention due to their different mechanisms of action (MoAs) in comparison to clinical platinum-based anticancer agents.[6−9] Most of these studies have focused on the synthesis and application of cationic and neutral complexes, in which a great number of bidentate XY ligands have been explored.[10−20] The Sadler group showed that the replacement of a neutral bipyridine ligand by the negatively charged anionic 2-phenylpyridine ligand in iridium(III) complexes can switch on biological activity (Scheme 1, **I** and **II**).[21−23] In addition, our group has also found the effect of the counteranion on the biological activity for cationic half-sandwich iridium(III) complexes containing a bipyridine ligand (Scheme 1, **III**).[24] These studies suggest that the charge of the metal center, the bidentate ligands, and the nature of the counteranions have an important effect on their cytotoxicity. As a result, we subsequently reported a series of half-sandwich zwitterionic iridium(III) and ruthenium(II) complexes and compared their biological activity with the corresponding cationic complexes in an earlier communication (Scheme 1, **IV** and **V**).[25] The cationic complexes displayed promising activity toward cancer cells, while the zwitterionic complexes were inactive. This different biological behavior may be primarily due to the different hydrophobicities between zwitterionic and cationic complexes. Thus, this prompted us to increase the anticancer activity of these zwitterionic complexes by further structural modification.

Fluorine has been studied extensively in the rational design of organic anticancer drugs.[26−28] The introduction of fluorine into a molecule can increase potency and affect target selectivity by modulating the conformation and affecting the pK_a, lipophilicity, and hydrophobic interactions.[29] However, to the best of our knowledge, the strategic incorporation of fluorine into transition-metal-based complexes to improve

Received: October 11, 2019

DOI: 10.1021/acs.inorgchem.9b03006
Inorg. Chem. XXXX, XXX, XXX−XXX

Scheme 1. Reported Half-Sandwich Iridium(III) Complexes and Our Current Work

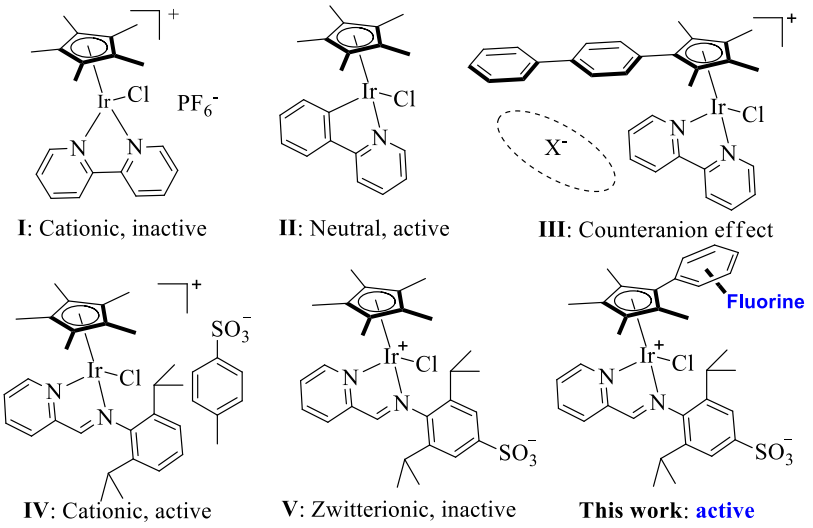

Scheme 2. Synthesis of Complexes Ir1−Ir7

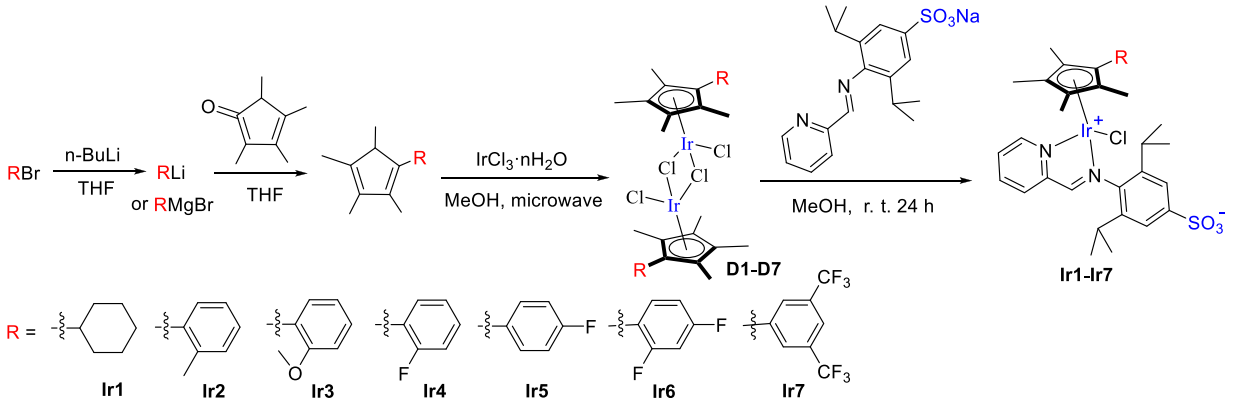

their potency has been rarely reported so far. A limited example has demonstrated that trifluoromethylation is a useful approach for influencing the pharmacological behavior of ruthenium(II) anticancer complexes.[30] Thus, we became interested in improving the anticancer activity of the aforementioned zwitterionic complexes through the strategy of fluorine substitution. On the basis of these considerations, we herein report the synthesis and characterization of a series of zwitterionic η^5-C_5Me_4R (Cp^R)-type iridium(III) complexes and explore the ligand substituent (especially fluorine substitution) effect on the anticancer activity of these complexes. Further, the chemical properties of these complexes, mechanisms of action, and molecular imaging in live cells have been systematically investigated. This work appears to be the first example of the fluorine effect in iridium-based anticancer complexes.

RESULTS AND DISCUSSION

Synthesis, Characterization, and Spectroscopic Properties. A sulfonated iminopyridine ligand was prepared using the literature procedure.[25] As shown in Scheme 2, the modified cyclopentadienyl-type ligands HCp^R (Cp^R = C_5Me_4R; R = Cy, 2-methylbenzene, 2-methoxybenzene, 2-fluorobenzene, 4-fluorobenzene, 2,4-difluorobenzene, 3,5-bis-(trifluoromethyl)benzene) were synthesized via the reaction of RLi (formed in situ by the reaction of *n*-BuLi with the respective bromides) or Grignard reagents and 2,3,4,5-tetramethyl-2-cyclopentenone in anhydrous THF, followed by elimination of water under acidic conditions. The chloro-bridged iridium dimer complexes $[(\eta^5\text{-}Cp^R)IrCl_2]_2$ were then obtained by the microwave-assisted reaction of HCp^R with $IrCl_3(H_2O)_n$. Subsequently, treatment of $[(\eta^5\text{-}Cp^R)IrCl_2]_2$ (**D1−D7**) with a sulfonated iminopyridine ligand in methanol at room temperature gave access to complexes **Ir1−Ir7** in moderate isolated yields (53.9−77.5%). These complexes were fully characterized by NMR spectroscopy (Figures S1−S18), elemental analysis, mass spectrometry (Figures S19−S29), and X-ray crystallography.

Single-crystals of **Ir1−Ir4** and **Ir7** suitable for X-ray diffraction analysis were obtained by slow diffusion of Et_2O into the iridium(III) complex solution in methanol or slow evaporation of the methanol and CH_2Cl_2 solution mixture at room temperature (Tables S1 and S2). The molecular structures of **Ir1−Ir4** and **Ir7** are shown in Figure 1. These complexes exhibit the expected "three-legged piano-stool" pseudo-octahedral half-sandwich structure. The cationic iridium center is connected covalently through the iminopyridine ligand to a terminal negative sulfonate group. In addition, intermolecular $\pi-\pi$ stacking in the unit cell was not observed in these crystal structures. In the solid state, **Ir2** adopts a conformation with the methyl group (C30) above the tetramethylcyclopentadienyl ring (far from the iridium

DOI: 10.1021/acs.inorgchem.9b03006
Inorg. Chem. XXXX, XXX, XXX−XXX

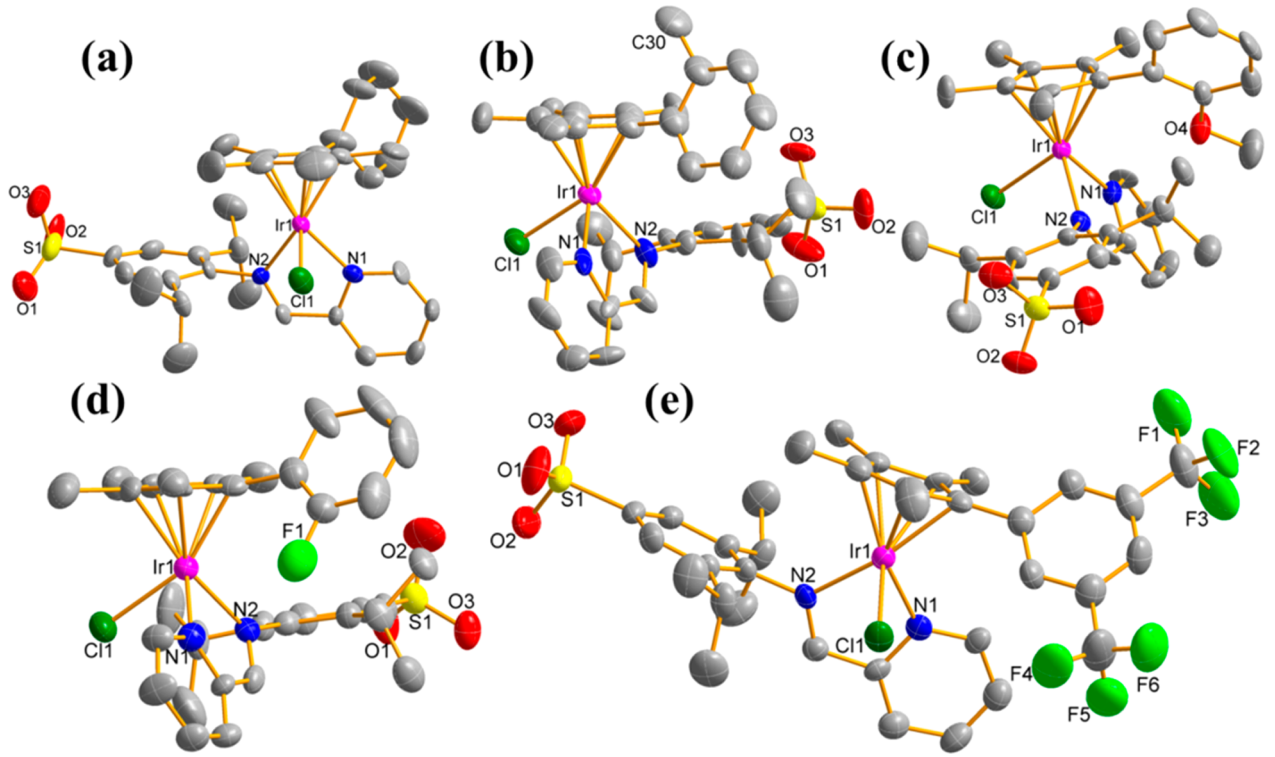

Figure 1. X-ray crystal structures with atom-numbering schemes for (a) complex **Ir1**, (b) complex **Ir2**, (c) complex **Ir3**, (d) complex **Ir4**, and (e) complex **Ir7** with thermal ellipsoids drawn at the 50% probability level. The hydrogen atoms have been omitted for clarity.

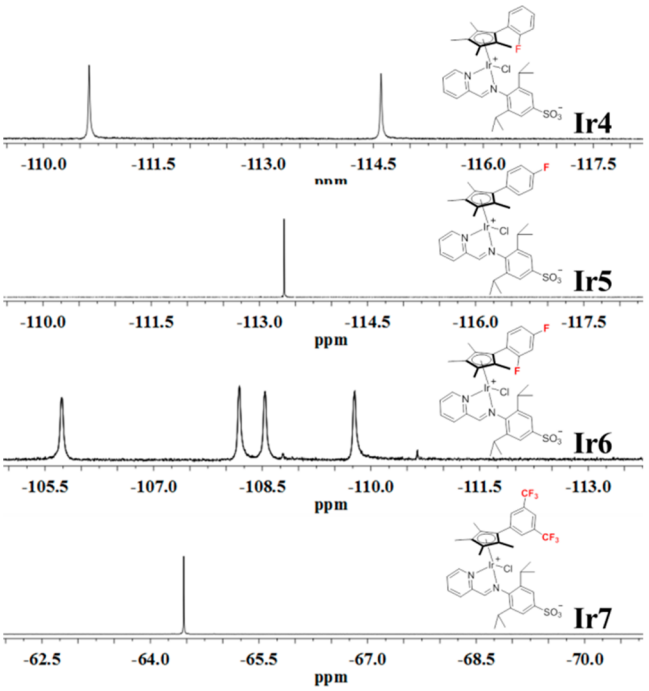

Figure 2. ^{19}F NMR spectrum of the fluoro complexes **Ir4**−**Ir7**.

center) while **Ir3** and **Ir4** adopt a conformation with the methoxyl and fluorine groups below the tetramethylcyclopentadienyl ring (close to the iridium center), respectively. Interestingly, ^{19}F NMR analysis clearly showed that the one fluorine group of **Ir4** and the two fluorine groups of **Ir6** give rise to two and four singlets (Figure 2), respectively, indicating that the asymmetrically substituted fluoro complexes **Ir4** and **Ir6** in the CD_3OD solution exist as two conformational isomers arising from C(cyclopentadienyl)−C(aryl) rotation. It may be difficult for the small fluorine groups to completely prohibit this rotation, allowing the isomerization to occur on the NMR time scale. This identification was further supported by the ^{19}F NMR spectrum of symmetrically substituted fluoro complexes **Ir5** and **Ir7**, where only one singlet was observed (Figure 2).

UV/vis absorption spectra of **Ir1**−**Ir7** were obtained in CH_2Cl_2 solution (final DMSO concentration, 1% v/v) (Figure 3a). Complexes **Ir1**−**Ir7** exhibited one sharp band maximum at ca. 285 nm (ε at the order of 10^3 M^{-1} cm^{-1}) and two broad and weak band maxima at ca. 380 and 480 nm, respectively. The substitution pattern of the cyclopentadienyl ring seems to have no notable effect on the absorption properties. Emission wavelengths of **Ir1**−**Ir7** were also determined at 25 °C in CH_2Cl_2 solutions (Figure 3b). Upon excitation at 315 nm, **Ir1**−**Ir7** showed emission bands with emission maxima between 406 and 425 nm. It seems that the ligand structure has little influence on the emission wavelength of these iridium(III) complexes. Notably, many advantages of the fluorescent complexes are expected: information on the accumulation, uptake, and distribution of the anticancer agents in living cells could be more easily obtained using fluorescence or confocal microscopy instrumentation.[31,32] Thus, the fluorescent property of half-sandwich zwitterionic iridium(III) complexes in this system represents a big advantage and is capable of providing a tool to get further insight into MoAs of these anticancer complexes.

Stability in Solution. The stability of the complexes under aqueous and physiological conditions plays a key role in the development of drugs. The stability of the complexes **Ir4**−**Ir7** in 80% DMSO-d_6/20% phosphate-buffered saline (PBS) (pH ∼7.2, PBS is prepared from D_2O) was monitored by ^{1}H NMR at 37 °C. The presence of DMSO can enhance the

DOI: 10.1021/acs.inorgchem.9b03006
Inorg. Chem. XXXX, XXX, XXX−XXX

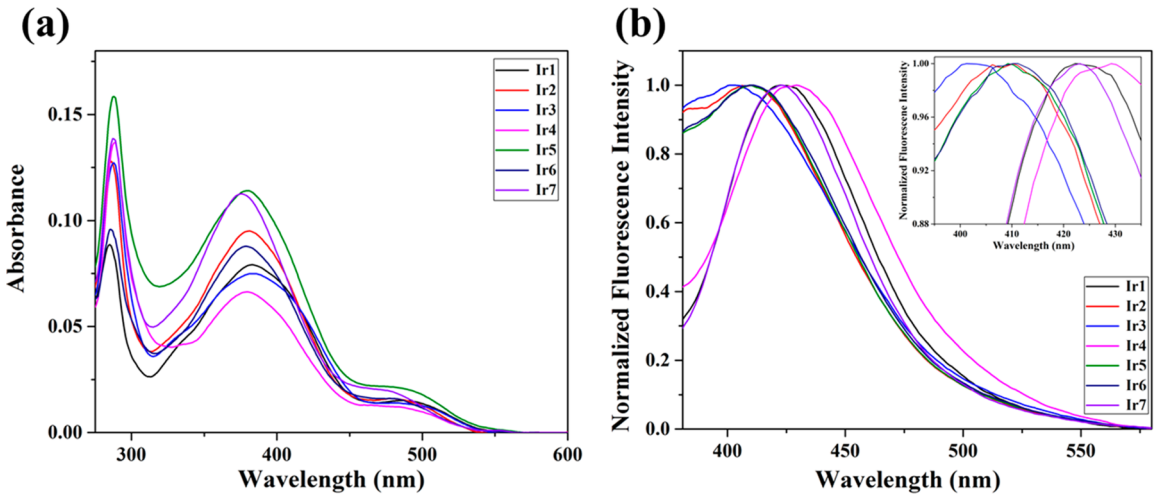

Figure 3. (a) UV/vis spectra of complexes **Ir1**−**Ir7** (20 μM) in CH_2Cl_2 at 25 °C. (b) Normalized emission spectra of complexes **Ir1**−**Ir7** (20 μM) in CH_2Cl_2 at 25 °C (λ_{ex} = 315 nm). The inset represents the locally enlarged spectra for clarity.

Table 1. IC_{50} Values of Complexes Ir1−Ir7 Tested toward Cancer and Normal Cell Lines and Comparison with Cisplatin

	IC_{50} (μM)			
complex	A549	HeLa	HepG2	BEAS-2B
Ir1	167.0 ± 2.7	164.0 ± 3.0	183.2 ± 2.1	
Ir2	182.5 ± 3.1	177.5 ± 3.5	175.0 ± 2.8	
Ir3	193.4 ± 2.5	173.5 ± 2.7	179.3 ± 3.2	
Ir4	38.6 ± 0.5	35.6 ± 1.8	34.6 ± 1.1	58.8 ± 1.7
Ir5	50.5 ± 0.7	32.6 ± 1.4	35.7 ± 0.9	82.1 ± 2.0
Ir6	50.3 ± 1.2	41.1 ± 1.7	46.9 ± 1.3	82.6 ± 1.5
Ir7	51.0 ± 0.8	33.1 ± 1.0	34.8 ± 0.9	57.8 ± 0.9
cisplatin	21.3 ± 1.7	7.5 ± 0.2	22.7 ± 1.1	42.0 ± 2.3

solubility of these complexes. The ^{1}H NMR spectra of **Ir4**−**Ir7** showed no change over a period of 24 h, and the assignment of the peaks was fully consistent with their structures (Figures S30−S33), indicating that **Ir4**−**Ir7** did not suffer from decomposition or ligand dissociation under these conditions. Previous studies showed that some cationic and neutral iridium(III) or ruthenium(II) complexes may be unstable in solutions with a higher relative content of water.[20,33,34] Thus, complexes **Ir1**-**Ir7** were also evaluated over 8 h by UV−visible spectroscopy in a 10% DMSO/90% PBS (v/v) buffer mixture to further investigate the stability of these complexes in dilute solutions (Figure S34). The spectra of **Ir1**−**Ir7** exhibited only little or no change with time, thereby indicating their sufficient stability when a high content of water was employed. Overall, these results clearly indicated that the zwitterionic complexes in this system are stable for further investigation of chemical reactivity and biological activity.

In Vitro Cytotoxicity. The ability of all complexes **Ir1**−**Ir7** and the control compound cisplatin to inhibit cell growth was evaluated against three cancer cell lines, namely A549, HeLa, and hepatoma cell lines, which are representatives of the most common cancers. The cytotoxicity was determined by an MTT assay after 48 h of exposure to the complexes. The IC_{50} values (concentration at which 50% of the cell growth is inhibited) are summarized in Table 1. Complexes **Ir1**−**Ir3** were inactive (IC_{50} > 100 μM) against all cell lines, which reinforces our observations in an earlier communication.[25] The presence of aliphatic ring substituents and phenyl rings on the cyclopentadienyl ring did not increase the cytotoxicity. Very interestingly, complexes **Ir4**−**Ir7** exhibited cytotoxic behaviors toward A549, HeLa, and hepatoma cells

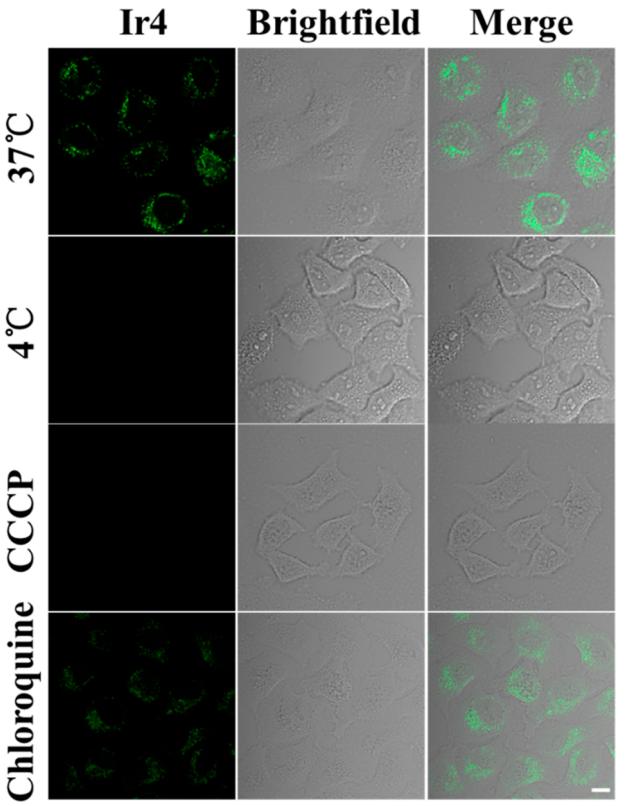

Figure 4. Cellular uptake mechanisms of complex **Ir4**. Confocal images of A549 cells after incubation with complex **Ir4** (2 μM) under different conditions: (top) cells were incubated with complex **Ir4** at 37 °C for 1 h (this served as a control); (second from top) cells were incubated with complex **Ir4** at 4 °C for 1 h; (third from top) cells were preincubated with the metabolic inhibitor CCCP (50 μM) at 37 °C for 1 h and then incubated with complex **Ir4** at 37 °C for 1 h; (bottom) cells were preincubated with chloroquine (50 μM) for 1 h at 37 °C and then incubated with complex **Ir4** at 37 °C for 1 h. λ_{ex} = 405 nm and λ_{em} = 430−490 nm. Scale bar: 20 μm.

DOI: 10.1021/acs.inorgchem.9b03006
Inorg. Chem. XXXX, XXX, XXX−XXX

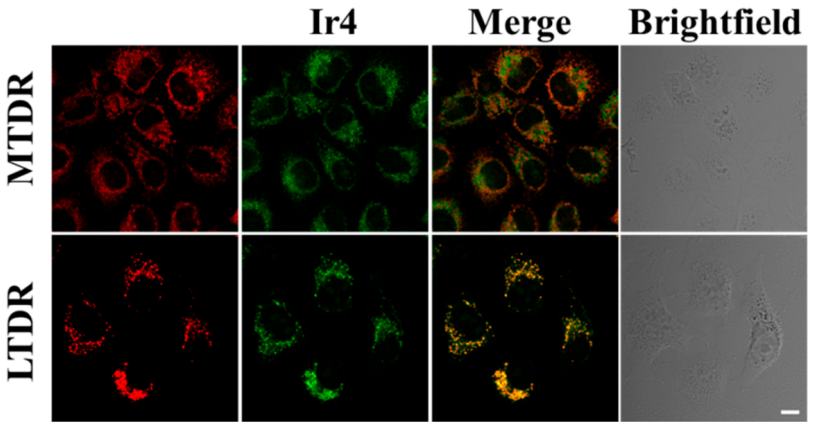

Figure 5. Determination of intercellular localization of **Ir4** by confocal microscopy. A549 cells were incubated with **Ir4** (2 μM) for 1 h at 37 °C and then coincubated with MTDR (500 nM) and LTDR (75 nM) for 1 h, respectively. **Ir4** was excited at 405 nm, and the emission was collected at 430−580 nm. MTDR was excited at 644 nm ,and the emission was collected at 660−720 nm. LTDR was excited at 594 nm, and the emission was collected at 600−660 nm. Scale bar: 20 μm.

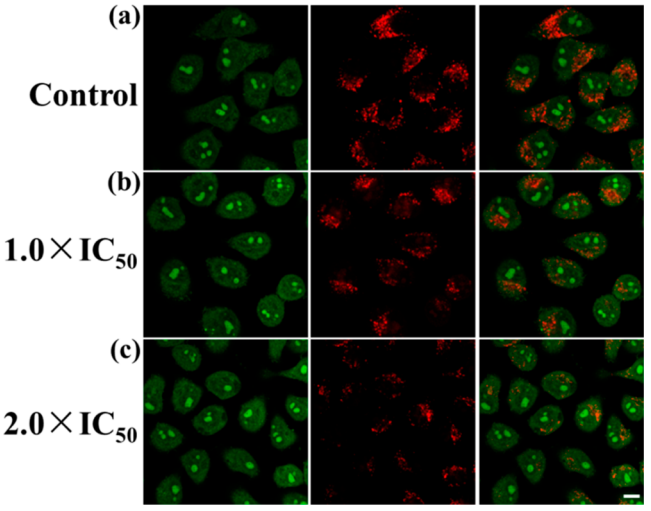

Figure 6. Observation of lysosomal disruption in A549 cells loaded with **Ir4** for 12 h at 37 °C and then stained with AO (5 μM) at 37 °C for 15 min. AO green fluorescence: λ_{ex} = 488 nm and λ_{em} = 510 ± 20 nm. AO red fluorescence: λ_{ex}= 488 nm and λ_{em} = 625 ± 20 nm. Scale bar: 20 μm. The cells were treated with (a) only acridine orange (AO), (b) acridine orange (AO) and **Ir4** (1.0 × IC_{50}), and (c) acridine orange (AO) and **Ir4** (2.0 × IC_{50}).

with IC_{50} values of 38.6−51.0, 32.6−41.1, and 34.6−46.9 μM, respectively. A comparison of IC_{50} values of **Ir1**−**Ir3** and of **Ir4**−**Ir7** reveals the tendency that the presence of fluorinated substituents in the η^5-Cp^R ring for these complexes gives rise to a significant increase (ca. 4 times) in the anticancer activity. Notably, the IC_{50} values of the complexes were not sensitive to the type of fluorinated substituent (**Ir4**−**Ir6** vs **Ir7**) as well as its number (**Ir4** and **Ir5** vs **Ir6**) and position (**Ir4** vs **Ir5**). However, the complexes in this system showed slightly lower activity than the clinical drug cisplatin against these three cancer cell lines. The cytotoxic activities of **Ir4**−**Ir7** against the normal cell line BEAS-2B (human bronchial epithelial cells) were also further determined (Table 1). Unfortunately, weak selectivity was observed for cancer cells versus normal cells with these complexes.

Lipophilicity and Cellular Uptake. The hydrophobicity of complexes is considered to be a key factor related to cellular uptake and their anticancer activity. Hence, the octanol/water partition coefficients (log *P*) for these complexes was determined by the shake-flask method (Figures S35−S41). The log *P* value revealed the following trend in lipophilicity: **Ir7** (1.43) > **Ir6** (0.77) > **Ir4** (0.74) > **Ir5** (0.61) > **Ir1** (0.42) > **Ir3** (0.35) ≈ **Ir2** (0.34). Clearly, the introduction of fluorinated substituents enhanced the lipophilicity of these zwitterionic complexes (**Ir4**−**Ir7** vs **Ir1**−**Ir3**). Because lipophilicity has often correlated with cell uptake and anticancer activity, the total cellular accumulation of these complexes was also investigated by ICP-MS after 48 h of exposure to these zwitterionic complexes (5 μM) (Figure S42). The intracellular iridium contents were in the following order: **Ir7** (0.573 ng/μg protein) > **Ir6** (0.566 ng/μg protein) > **Ir4** (0.548 ng/μg protein) > **Ir5** (0.531 ng/μg protein) > **Ir3** (0.272 ng/μg protein) > **Ir1** (0.235 ng/μg protein) > **Ir2** (0.220 ng/μg protein). Basically, the lipophilicity of these complexes was correlated with their cellular uptake level. However,the four fluoro complexes exhibited comparable cellular uptake efficiencies (0.531−0.573 ng/μg protein), which was consistent with their similar cytotoxicities (38.6−51.0, 32.6−41.1, and 34.6−46.9 μM). In addition, complexes **Ir4**−**Ir7** showed a ca. 2.5-fold higher cellular iridium accumulation in comparison to complexes **Ir1**−**Ir3**. Overall, thefluoro complexes **Ir4**−**Ir7** gave rise to an increased hydrophobicity in comparison to **Ir1**−**Ir3**, leading to a significantly increased cell uptake and anticancer activity. As a result, the lipophilicity and cellular uptake levels of these complexes appeared to be the primary factors for their cytotoxicity in this system.

Due to the luminescent properties of these complexes, we also investigated the cellular uptake mechanism of **Ir4** by confocal microscopy. Clear confocal microscopy images were observed for **Ir4** at λ_{ex} = 405 nm at 37 °C (Figure 4). The punctate green fluorescence in the cytoplasm suggested that **Ir4** can effectively penetrate into A549 cells after 1 h of incubation. Generally, small molecules can enter cells through energy-independent (passive diffusion and facilitated diffusion) or energy-dependent (active transport and endocytosis) transport pathways. Incubation of A549 cells with **Ir4** at 4 °C or in the presence of the metabolic inhibitor carbonyl cyanide 3-chlorophenylhydrazone (CCCP) led to a significant decrease in intracellular luminescence in comparison to the control cells incubated at 37 °C. However, no obvious change

DOI: 10.1021/acs.inorgchem.9b03006
Inorg. Chem. XXXX, XXX, XXX−XXX

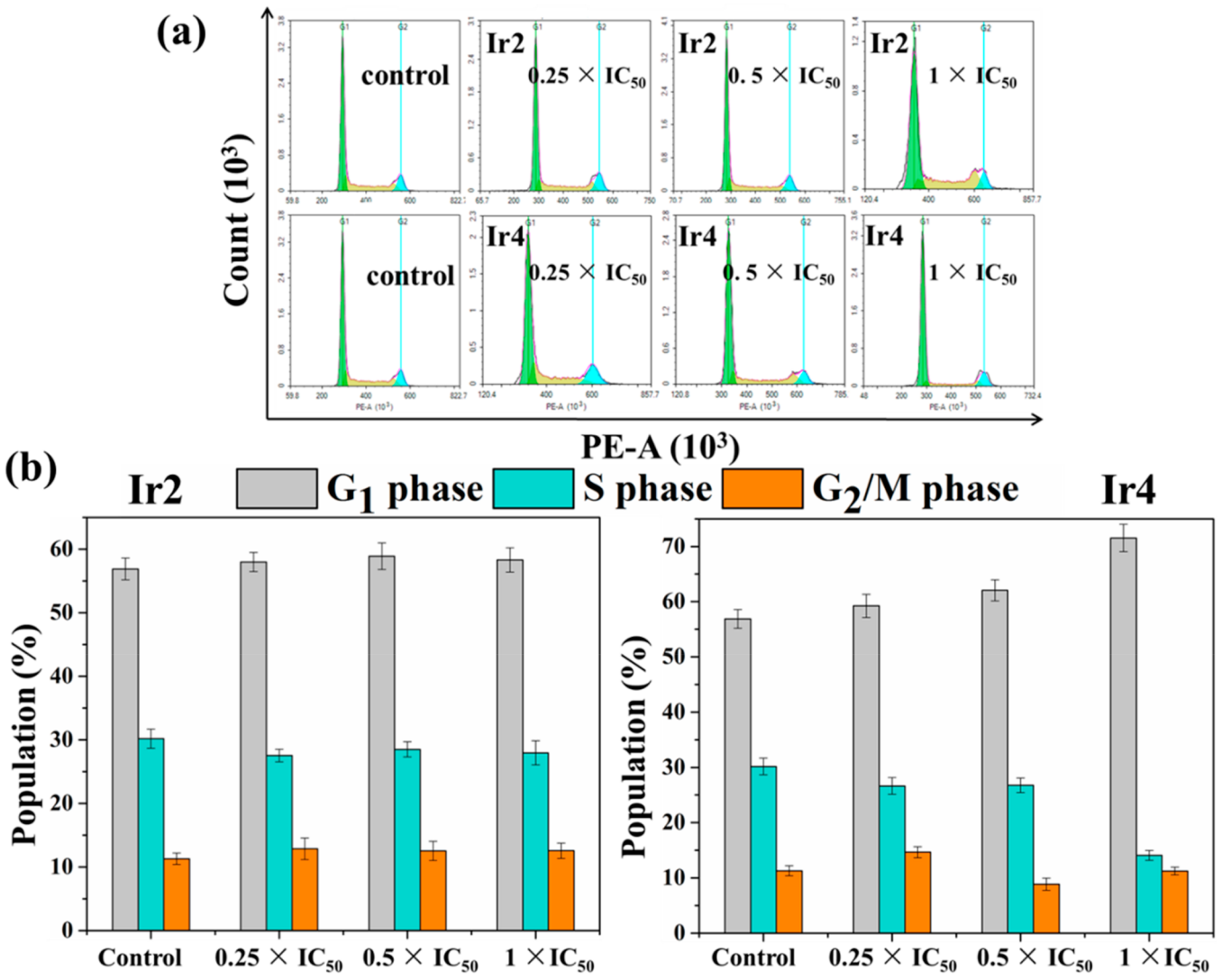

Figure 7. Cell cycle analysis of A549 cells after 48 h of exposure to complexes **Ir2** and **Ir4** at 37 °C. The concentrations used were 0.25, 0.5, and 1 equipotent concentrations of IC_{50}. Cell staining for flow cytometry was carried out using PI/RNase. (a) FL2 histogram for the negative control (untreated cells), **Ir2**, and **Ir4** with 0.25, 0.5, and 1 equipotent concentrations of IC_{50}. (b) Cell populations in each cell-cycle phase for control, **Ir2**, and **Ir4**. Data are quoted as mean ± SD of three replicates.

in the luminescent intensity in the chloroquine (endocytosis inhibitor) group was detected in comparison to the control groups. Thus, these zwitterionic complexes were transported into A549 cells mainly through a well-known energy-dependent pathway, e.g. via active transport, and endocytosis was not responsible for their uptake, which followed the behavior of our previously reported cationic iridium(III) and ruthenium(II) complexes containing the iminopyridyl ligands.[35]

Cellular Localization. To determine which organelles would be targeted by these zwitterionic complexes, the A549 cells were dual-stained with **Ir4** and the organelle-specific probe LysoTracker Deep Red (LTDR) or MitoTracker Deep Red (MTDR), respectively. Subsequently, colocalization analysis was performed by confocal microscopy. As shown in Figure 5, the organelle-specific stain for lysosome displayed good concordance between overlay images of **Ir4** and LTDR in A549 cancer cells. A Pearson correlation coefficient (PCC) of 0.77 (LTDR) in the merged image was observed for **Ir4**. However, negligible colocalization (PCC = −0.13) was observed for **Ir4** with the MTDR. These results suggested that **Ir4** can selectively localize in the lysosome and the cytotoxicity of these zwitterionic complexes may arise from lysosome-mediated cell death.

Lysosomal Damage. To further investigate lysosome-mediated cell death, the lysosomal integrity of A549 cells was also determined by acridine orange (AO) staining using confocal microscopy. AO is an effective probe that is widely used to investigate the integrity of the acidic organelles, since it emits red fluorescence in lysosomes and green fluorescence in cytosol or nuclei.[36−38] As expected, A549 cancer cells treated with AO exhibited red fluorescence in lysosomes. Notably, the red fluorescence of AO significantly decreased with the increased concentration of **Ir4** (Figure 6), thereby suggesting that lysosomal integrity was jeopardized upon **Ir4** treatment. This result is consistent with the aforementioned selective accumulation of **Ir4** in the lysosome. Therefore, the fluoro zwitterionic complexes in this system may induce cell death via the disruption of lysosomes.

Cell-Cycle and Apoptosis Studies. To further determine the MoAs of these zwitterionic complexes, cell-cycle arrest analysis for the typical **Ir4** toward A549 cells was determined

DOI: 10.1021/acs.inorgchem.9b03006
Inorg. Chem. XXXX, XXX, XXX−XXX

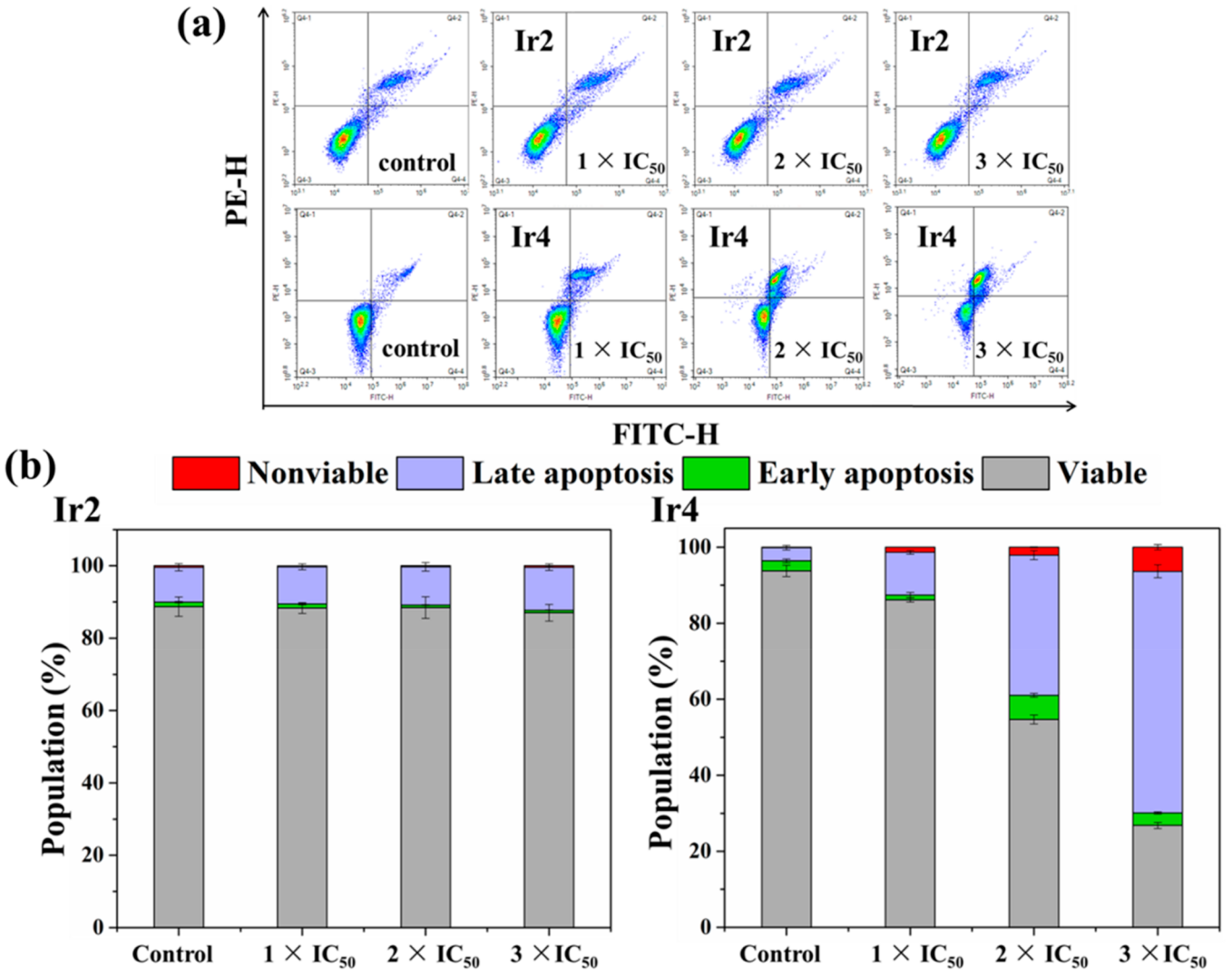

Figure 8. (a) Apoptosis analysis of A549 cells after 48 h of exposure to complexes **Ir2** and **Ir4** at 37 °C determined by flow cytometry using annexin V-FITC vs PI staining. (b) Histograms of apoptosis analysis for A549 cells after treatment with complexes **Ir2** and **Ir4**. Data are quoted as mean ± SD of three replicates.

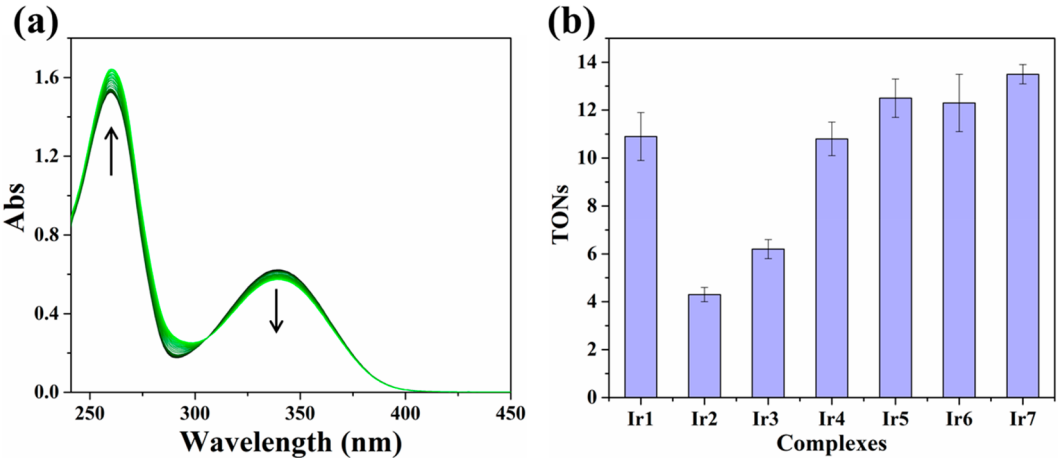

Figure 9. (a) UV/vis spectra of the reaction of NADH (100 μM) with complex **Ir4** (1 μM) in 20% DMSO/80% H_2O (v/v) at 37 °C for 8 h. (b) Turnover numbers (TONs) of complexes **Ir1**−**Ir7**. Data are quoted as mean ± SD of three replicates.

by flow cytometry (Figure 7 and Tables S3 and S4). Treatment of A549 cancer cells with **Ir4** at 0.25, 0.5, and 1 equipotent concentrations of IC_{50} for 48 h led to G_1 phase arrest, where the percentages of cells increased by 25.8% at 1 × IC_{50} concentration in comparison to the untreated control cells. These result suggested that complex **Ir4** stopped the cell

DOI: 10.1021/acs.inorgchem.9b03006
Inorg. Chem. XXXX, XXX, XXX−XXX

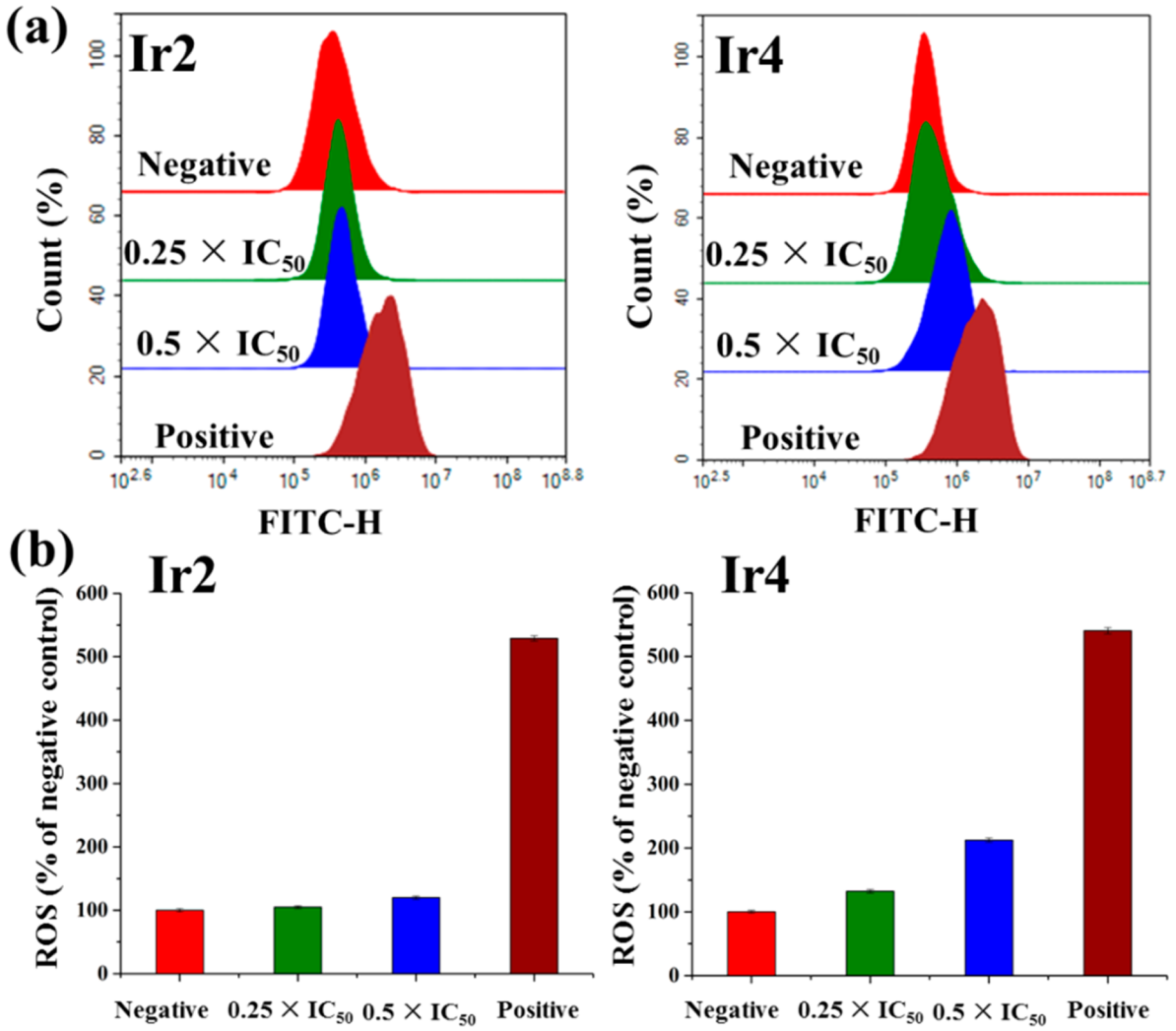

Figure 10. Analysis of ROS level by flow cytometry after A549 cells were treated with es **Ir2** and **Ir4** at the 0.25 and 0.5 equipotent concentrations of IC_{50} for 48 h and stained with H_2DCFDA. Data are quoted as mean ± SD of three replicates.

cycle mainly at the G_1 phase in a concentration-dependent manner. In contrast, treatment of A549 cells with complex **Ir2** at 0.25, 0.5, and 1 × IC_{50} concentration led to a negligible change of the cell-cycle progression in comparison to untreated cells.

To understand if the decrease in A549 cell viability in the presence of the active complexes is due to the induction of apoptosis, cells were exposed to **Ir4** at concentrations of 1, 2, and 3 equipotent concentrations of IC_{50} for 48 h and then analyzed by flow cytometry (Figure 8 and Table S5). Clearly, a concentration-dependent apoptosis population was observed for **Ir4** and most of the apoptotic cells were in the late apoptosis stage. For example, at 3 × IC_{50} concentration, a total of 66.9% of early apoptotic (3.3%) and late apoptotic (63.6%) cells were undergoing increased apoptosis in comparison to the untreated control (6.2%). On the other hand, complex **Ir2** without fluorine led to negligible changes in the apoptosis against A549 cancer cells under the same test conditions, which is in agreement with its relatively low cytotoxicity (Table S6). Thus, these fluoro zwitterionic complexes can induce cell death through the apoptotic pathway.

Catalysis of NADH Oxidation. The coenzymes nicotinamide adenine dinucleotide (NADH) and NAD^+ play an important role in many biocatalyzed processes. Previous work has shown that some neutral half-sandwich iridium(III) anticancer complexes are capable of oxidizing NADH by hydride transfer to the metal center and generate reactive oxygen species (ROS) in the form of H_2O_2.[39,40] Thus, we also investigated whether these zwitterionic complexes had the same property. The transfer hydrogenation reactions between NADH (100 μM) and **Ir1**−**Ir7** (ca. 1 μM) in 20% DMSO/80% H_2O (v/v) were monitored by UV−vis spectroscopy over a period of 8 h (Figure 9a and Figure S43). The absorbance at 339 nm decreased while the absorbance at 260 nm increased. This is typical of the conversion of NADH to NAD^+. The turnover numbers (TONs) of **Ir1** (10.9), **Ir2** (4.3), **Ir3** (6.2), **Ir4** (10.8), **Ir5** (12.5), **Ir6** (12.2), and **Ir7** (13.5) were calculated by measuring the absorption difference at 339 nm (Figure 9b). The basic trend that the introduction of the fluorinated substituents in the η^5-Cp^R ring enhanced the catalytic activity (**Ir2** and **Ir3** vs **Ir4**−**Ir7**) was observed. However, the turnover numbers (TONs) are not fully correlated with their cytotoxicity. It seemed that the catalytic activity of NADH oxidation is due not only to electronic effects of the substituents on the aryl ring (**Ir2**−**Ir7**), but also conjugation effect (**Ir1** vs **Ir2**−**Ir7**) in the molecular structures. The catalytic transfer hydrogenation may provide

DOI: 10.1021/acs.inorgchem.9b03006
Inorg. Chem. XXXX, XXX, XXX−XXX

a potential pathway to induce reactive oxygen species (ROS) and enhance the killing of cancer cells in an oxidant mechanism of action.[40] However, the TONs of these complexes cannot fully explain the difference in IC_{50} values among these complexes.

Intracellular ROS Level Determination. The generation of ROS, which often leads to many related protein expressions and induces apoptosis, is a well-known MoA of anticancer complexes.[41−46] High concentrations of ROS often lead to oxidative stress and damage to cancer cells.[40,47] The oxidation of NADH is one of the pathways to produce the ROS.[40] Thus, the effect of **Ir2** and **Ir4** on intracellular ROS levels in A549 cancer cells was determined by flow cytometry analysis. Generally, a higher level of iridium accumulation would enhance the catalysis of NADH oxidation in cancer cells and could be the main factor to influence the ROS levels in cancer cells. As expected, fluoro complex **Ir4** with the higher iridium accumulation showed higher ROS total levels in comparison to **Ir2** under the same test conditions (Figure 10). In addition, **Ir4** can induce ROS overproduction in a dose-dependent manner. These results indicated that elevated levels of ROS may be responsible for the cytotoxicity of these fluoro zwitterionic iridium(III) complexes. It should be noted that some neutral half-sandwich iridium(III) complexes bearing C,N-chelated ligands could generate ROS by catalytic hydride transfer from the coenzyme NADH to oxygen.[40] Similarly, the generation of ROS for these complexes may arise from the catalytic conversion of NADH to NAD^+, which was also observed in this system. As a result, the increased ROS level was also deemed as one of the MoAs for **Ir4**. It has been shown that excessive ROS can activate the NF-κB channel.[45] Thus, the NF-κBp65 protein count in the cells exposed to the complex was determined by flow cytometry (Figure S44). In comparison with the control group, the content of NF-κBp65 protein in the cells with **Ir4** at 1 × IC_{50} concentration increased significantly. Furthermore, the NF-κB activation induced by **Ir4** was repressed by the treatment of NAC (*N*-acetylcysteine, a known antioxidant). These results suggested that NF-κB activity was increased by ROS regulation, and apoptosis through a ROS-NF-κB signaling pathway.

CONCLUSIONS

In conclusion, seven zwitterionic half-sandwich iridium(III) complexes containing different substituents in the η^5-Cp^R ring have been synthesized and fully characterized. Two conformational isomers arising from C(cyclopentadienyl)−C(aryl) rotation were observed in CD_3OD solution for the asymmetrically substituted fluoro complexes **Ir4** and **Ir6.** These complexes are very stable in aqueous solution and have a detectable fluorescence. In addition, they can catalyze oxidation of NADH to NAD^+. Most interestingly, the structure−activity relationships in this system are very significant. The presence of the fluorinated substituents resulted in an increased hydrophobicity, thus leading to a significantly increased cellular accumulation and enhanced anticancer activity. Subsequently, the MoAs of the active zwitterionic complexes in this system were determined by confocal microscopy imaging and flow cytometry. The typical fluoro complex **Ir4** can be effectively and quickly taken into A549 cells through an energy-dependent pathway and was mainly located in lysosomes. Further, complex **Ir4** may induce apoptosis through lysosomal damage. On the other hand, complex **Ir4** arrested the cell cycle at thr G_1 phase, induced cell apoptosis (late apoptosis stage predominates), and promoted an increase in ROS level, which may provide a basis for killing cancer cells. This work demonstrates that the rational chemical design arising from the strategic incorporation of fluorine in drug agents can also be applied to transition-metal-based anticancer complexes. This may provide an alternative strategy for further development of a new class of anticancer complexes.

ASSOCIATED CONTENT

Supporting Information

The Supporting Information is available free of charge at https://pubs.acs.org/doi/10.1021/acs.inorgchem.9b03006.

Experimental section and figures and tables as detailed in the text (PDF)

Accession Codes

CCDC 1887368, 1887374−1887375, 1887999, and 1941647 contain the supplementary crystallographic data for this paper. These data can be obtained free of charge via www.ccdc.cam.ac.uk/data_request/cif, or by emailing data_request@ccdc.cam.ac.uk, or by contacting The Cambridge Crystallographic Data Centre, 12 Union Road, Cambridge CB2 1EZ, UK; fax: +44 1223 336033.

AUTHOR INFORMATION

Corresponding Authors

*E-mail for L.G.: guolihua@qfnu.edu.cn.
*E-mail for Z.L.: liuzheqd@163.com.

ORCID

Lihua Guo: 0000-0002-0842-9958
Zhe Liu: 0000-0001-5796-4335

Notes

The authors declare no competing financial interest.

ACKNOWLEDGMENTS

We thank Shandong Provincial Natural Science Foundation (ZR2018MB023), Young Talents Invitation Program of Shandong Provincial Colleges and Universities, the National Natural Science Foundation of China (Grant No. 21671118), and the Taishan Scholars Program for support.

REFERENCES

(1) Kelland, L. The Resurgence of Platinum-Based Cancer Chemotherapy. *Nat. Rev. Cancer* **2007**, *7*, 573−584.
(2) Johnstone, T. C.; Suntharalingam, K.; Lippard, S. J. The Next Generation of Platinum Drugs: Targeted Pt(II) Agents, Nanoparticle Delivery, and Pt(IV) Prodrugs. *Chem. Rev.* **2016**, *116*, 3436−3486.
(3) Hartinger, C. G.; Dyson, P. J. Bioorganometallic Chemistry—From Teaching Paradigms to Medicinal Applications. *Chem. Soc. Rev.* **2009**, *38*, 391−401.
(4) Bergamo, A.; Gaiddon, C.; Schellens, J. H. M.; Beijnen, J. H.; Sava, G. Approaching Tumour Therapy Beyond Platinum Drugs: Status of The Art and Perspectives of Ruthenium Drug Candidates. *J. Inorg. Biochem.* **2012**, *106*, 90−99.
(5) Barry, N. P. E.; Sadler, P. J. 100 Years of Metal Coordination Chemistry: From Alfred Werner to Anticancer Metallodrugs. *Pure Appl. Chem.* **2014**, *86*, 1897−1910.
(6) Liu, Z.; Sadler, P. J. Organoiridium Complexes: Anticancer Agents and Catalysts. *Acc. Chem. Res.* **2014**, *47*, 1174−1185.
(7) Soldevila-Barreda, J. J.; Romero-Canelón, I.; Habtemariam, A.; Sadler, P. J. Transfer Hydrogenation Catalysis in Cells as a New Approach to Anticancer Drug Design. *Nat. Commun.* **2015**, *6*, 6582.

DOI: 10.1021/acs.inorgchem.9b03006
Inorg. Chem. XXXX, XXX, XXX−XXX

(8) Konkankit, C. C.; Marker, S. C.; Knopf, K. M.; Wilson, J. J. Anticancer Activity of Complexes of The Third Row Transition Metals, Rhenium, Osmium, And Iridium. *Dalton Trans.* **2018**, *47*, 9934−9974.
(9) Zeng, L.; Gupta, P.; Chen, Y.; Wang, E.; Ji, L.; Chao, H.; Chen, Z.-S. The Development of Anticancer Ruthenium(II) Complexes: From Single Molecule Compounds to Nanomaterials. *Chem. Soc. Rev.* **2017**, *46*, 5771−5804.
(10) Yang, Y.; Guo, L.; Tian, Z.; Gong, Y.; Zheng, H.; Zhang, S.; Xu, Z.; Ge, X.; Liu, Z. Novel and Versatile Imine-N-Heterocyclic Carbene Half-Sandwich Iridium(III) Complexes as Lysosome-Targeted Anticancer Agents. *Inorg. Chem.* **2018**, *57*, 11087−11098.
(11) Du, Q.; Guo, L.; Tian, M.; Ge, X.; Yang, Y.; Jian, X.; Xu, Z.; Tian, Z.; Liu, Z. Potent Half-Sandwich Iridium(III) and Ruthenium-(II) Anticancer Complexes Containing a P̂O-Chelated Ligand. *Organometallics* **2018**, *37*, 2880−2889.
(12) Ludwig, G.; Kaluđerović, G. N.; Rüffer, T.; Bette, M.; Korb, M.; Block, M.; Paschke, R.; Lang, H.; Steinborn, D. Cationic Arene Ruthenium(II) Complexes With Chelating P-Functionalized Alkyl Phenyl Sulfide and Sulfoxide Ligands as Potent Anticancer Agents. *Dalton Trans.* **2013**, *42*, 3771−3774.
(13) Du, Q.; Zhao, L.; Guo, L.; Ge, X.; Zhang, S.; Xu, Z.; Liu, Z. Lysosome-targeted Cyclometalated Iridium (III) Anticancer Complexes Bearing Phosphine-Sulfonate Ligands. *Appl. Organomet. Chem.* **2019**, *33*, No. e4746.
(14) Ludwig, G.; Mijatović, S.; Ranđelović, I.; Bulatović, M.; Miljković, D.; Maksimović-Ivanić, D.; Korb, M.; Lang, H.; Steinborn, D.; Kaluđerović, G. N. Biological Activity of Neutral and Cationic Iridium(III) Complexes With κP and κP,κS Coordinated $Ph_2PCH_2S(O)_xPh$ (x = 0−2) ligands. *Eur. J. Med. Chem.* **2013**, *69*, 216−222.
(15) Yang, Y.; Guo, L.; Tian, Z.; Liu, X.; Gong, Y.; Zheng, H.; Ge, X.; Liu, Z. Imine-N-Heterocyclic Carbenes as Versatile Ligands in Ruthenium(II) p-Cymene Anticancer Complexes: A Structure-Activity Relationship Study. *Chem. - Asian J.* **2018**, *13*, 2923−2933.
(16) Broomfield, L. M.; Alonso-Moreno, C.; Martin, E.; Shafir, A.; Posadas, I.; Ceña, V.; Castro-Osma, J. A. Aminophosphine Ligands as aPrivileged Platform for Development of Antitumoral Ruthenium(II) Arene Complexes. *Dalton Trans.* **2017**, *46*, 16113−16125.
(17) Du, Q.; Yang, Y.; Guo, L.; Tian, M.; Ge, X.; Tian, Z.; Zhao, L.; Xu, Z.; Li, J.; Liu, Z. Fluorescent Half-Sandwich Phosphine-Sulfonate Iridium(III) and Ruthenium(II) Complexes as Potential Lysosome-Targeted Anticancer Agents. *Dyes Pigm.* **2019**, *162*, 821−830.
(18) Yang, Y.; Guo, L.; Ge, X.; Shi, S.; Gong, Y.; Xu, Z.; Zheng, X.; Liu, Z. Structure-Activity Relationships for Highly Potent Half-Sandwich Organoiridium(III) Anticancer Complexes With ĈN-Chelated Ligands. *J. Inorg. Biochem.* **2019**, *191*, 1−7.
(19) Jeyalakshmi, K.; Haribabu, J.; Balachandran, C.; Swaminathan, S.; Bhuvanesh, N. S. P.; Karvembu, R. Coordination Behavior of N, N', N″-Trisubstituted Guanidine Ligands in Their Ru-Arene Complexes: Synthetic, DNA/Protein Binding, and Cytotoxic Studies. *Organometallics* **2019**, *38*, 753−770.
(20) Guo, L.; Zhang, H.; Tian, M.; Tian, Z.; Xu, Y.; Yang, Y.; Peng, H.; Liu, P.; Liu, Z. Electronic Effects on Reactivity and Anticancer Activity by Half-Sandwich N, N-Chelated Iridium(III) Complexes. *New J. Chem.* **2018**, *42*, 16183−16192.
(21) Liu, Z.; Salassa, L.; Habtemariam, A.; Pizarro, A. M.; Clarkson, G. J.; Sadler, P. J. Contrasting Reactivity and Cancer Cell Cytotoxicity of Isoelectronic Organometallic Iridium(III) Complexes. *Inorg. Chem.* **2011**, *50*, 5777−5783.
(22) Liu, Z.; Habtemariam, A.; Pizarro, A. M.; Fletcher, S. A.; Kisova, A.; Vrana, O.; Salassa, L.; Bruijnincx, P. C. A.; Clarkson, G. J.; Brabec, V.; Sadler, P. J. Organometallic Half-Sandwich Iridium Anticancer Complexes. *J. Med. Chem.* **2011**, *54*, 3011−3026.
(23) Liu, Z.; Habtemariam, A.; Pizarro, A. M.; Clarkson, G. J.; Sadler, P. J. Organometallic Iridium(III) Cyclopentadienyl Anticancer Complexes Containing C, N-Chelating Ligands. *Organometallics* **2011**, *30*, 4702−4710.
(24) Zhang, H.; Guo, L.; Tian, Z.; Tian, M.; Zhang, S.; Xu, Z.; Gong, P.; Zheng, X.; Zhao, J.; Liu, Z. Significant Effects of Counteranions on the Anticancer Activity of Iridium(III) complexes. *Chem. Commun.* **2018**, *54*, 4421−4424.
(25) Yang, Y.; Ge, X.; Guo, L.; Zhu, T.; Tian, Z.; Zhang, H.; Du, Q.; Peng, H.; Ma, W.; Liu, Z. Zwitterionic and Cationic Half-Sandwich Iridium(III)Ruthenium(II) Complexes Bearing Sulfonate Groups: Synthesis, Characterization and Their Different Biological Activities. *Dalton Trans.* **2019**, *48*, 3193−3197.
(26) Böhm, H.-J.; Banner, D.; Bendels, S.; Kansy, M.; Kuhn, B.; Müller, K.; Obst-Sander, U.; Stahl, M. Fluorine in Medicinal Chemistry. *ChemBioChem* **2004**, *5*, 637−643.
(27) Müller, K.; Faeh, C.; Diederich, F. Fluorine in Pharmaceuticals: Looking Beyond Intuition. *Science* **2007**, *317*, 1881−1886.
(28) Hagmann, W. K. The Many Roles for Fluorine in Medicinal Chemistry. *J. Med. Chem.* **2008**, *51*, 4359−4369.
(29) Gillis, E. P.; Eastman, K. J.; Hill, M. D.; Donnelly, D. J.; Meanwell, N. A. Applications of Fluorine in Medicinal Chemistry. *J. Med. Chem.* **2015**, *58*, 8315−8359.
(30) Chang, S. W.; Lewis, A. R.; Prosser, K. E.; Thompson, J. R.; Gladkikh, M.; Bally, M. B.; Warren, J. J.; Walsby, C. J. CF3 Derivatives of the Anticancer Ru(III) Complexes KP1019, NKP-1339, and Their Imidazole and Pyridine Analogues Show Enhanced Lipophilicity, Albumin Interactions, and Cytotoxicity. *Inorg. Chem.* **2016**, *55*, 4850−4863.
(31) Zimbron, J. M.; Passador, K.; Gatin-Fraudet, B.; Bachelet, C.-M.; Plażuk, D.; Chamoreau, L.-M.; Botuha, C.; Thorimbert, S.; Salmain, M. Synthesis, Photophysical Properties, and Living Cell Imaging of Theranostic Half-Sandwich Iridium-4,4-Difluoro-4-bora-3a,4a-diaza-s-indacene (BODIPY) Dyads. *Organometallics* **2017**, *36*, 3435−3442.
(32) Du, Q.; Guo, L.; Ge, X.; Zhao, L.; Tian, Z.; Liu, X.; Zhang, F.; Liu, Z. Serendipitous Synthesis of Five-Coordinated Half-Sandwich Aminoimine Iridium(III) and Ruthenium(II) Complexes and Their Application as Potent Anticancer Agents. *Inorg. Chem.* **2019**, *58*, 5956−5965.
(33) Biancalana, L.; Zacchini, S.; Ferri, N.; Lupo, M. G.; Pampaloni, G.; Marchetti, F. Tuning the Cytotoxicity of Ruthenium(II) Para-Cymene Complexes by Mono-Substitution at a Triphenylphosphine/Phenoxydiphenylphosphine Ligand. *Dalton Trans.* **2017**, *46*, 16589−16604.
(34) Snelders, D. J. M.; Casini, A.; Edafe, F.; van Koten, G.; Klein Gebbink, R. J. M.; Dyson, P. J. Ruthenium(II) Arene Complexes With Oligocationic Triarylphosphine Ligands: Synthesis, DNA Interactions and in Vitro Properties. *J. Organomet. Chem.* **2011**, *696*, 1108−1116.
(35) Li, J.; Guo, L.; Tian, Z.; Zhang, S.; Xu, Z.; Han, Y.; Li, R.; Li, Y.; Liu, Z. Half-Sandwich Iridium and Ruthenium Complexes: Effective Tracking in Cells and Anticancer Studies. *Inorg. Chem.* **2018**, *57*, 13552−13563.
(36) Boya, P.; Kroemer, G. Lysosomal membrane permeabilization in cell death. *Oncogene* **2008**, *27*, 6434.
(37) Yang, Y.; Guo, L.; Ge, X.; Tian, Z.; Gong, Y.; Zheng, H.; Du, Q.; Zheng, X.; Liu, Z. Novel Lysosome-targeted Cyclometalated Iridium(III) Anticancer Complexes Containing Imine-N-Heterocyclic Carbene Ligands: Synthesis, Spectroscopic Properties and Biological Activity. *Dyes Pigm.* **2019**, *161*, 119−129.
(38) Yang, Y.; Guo, L.; Tian, Z.; Ge, X.; Gong, Y.; Zheng, H.; Shi, S.; Liu, Z. Lysosome-Targeted Phosphine-Imine Half-Sandwich Iridium(III) Anticancer Complexes: Synthesis, Characterization, and Biological Activity. *Organometallics* **2019**, *38*, 1761−1769.
(39) Millett, A. J.; Habtemariam, A.; Romero-Canelón, I.; Clarkson, G. J.; Sadler, P. J. Contrasting Anticancer Activity of Half-Sandwich Iridium(III) Complexes Bearing Functionally Diverse 2-Phenylpyridine Ligands. *Organometallics* **2015**, *34*, 2683−2694.
(40) Liu, Z.; Romero-Canelón, I.; Qamar, B.; Hearn, J. M.; Habtemariam, A.; Barry, N. P. E.; Pizarro, A. M.; Clarkson, G. J.; Sadler, P. J. The Potent Oxidant Anticancer Activity of Organoiridium Catalysts. *Angew. Chem., Int. Ed.* **2014**, *53*, 3941−3946.
(41) Wu, K.-J.; Zhong, H.-J.; Yang, G.; Wu, C.; Huang, J.-M.; Li, G.; Ma, D.-L.; Leung, C.-H. Small Molecule Pin1 Inhibitor Blocking

DOI: 10.1021/acs.inorgchem.9b03006
Inorg. Chem. XXXX, XXX, XXX−XXX

NF-κB Signaling in Prostate Cancer Cells. *Chem. - Asian J.* **2018**, *13*, 275−279.
(42) Wu, K.-J.; Zhong, H.-J.; Li, G.; Liu, C.; Wang, H.-M. D.; Ma, D.-L.; Leung, C.-H. Structure-based identification of a NEDD8-activating enzyme inhibitor via drug repurposing. *Eur. J. Med. Chem.* **2018**, *143*, 1021−1027.
(43) Hsu, C.-C.; Lien, J.-C.; Chang, C.-W.; Chang, C.-H.; Kuo, S.-C.; Huang, T.-F. Yuwen02f1 suppresses LPS-induced endotoxemia and adjuvant-induced arthritis primarily through blockade of ROS formation, NFkB and MAPK activation. *Biochem. Pharmacol.* **2013**, *85*, 385−395.
(44) Huang, Q.; Zhan, L.; Cao, H.; Li, J.; Lyu, Y.; Guo, X.; Zhang, J.; Ji, L.; Ren, T.; An, J.; Liu, B.; Nie, Y.; Xing, J. Increased mitochondrial fission promotes autophagy and hepatocellular carcinoma cell survival through the ROS-modulated coordinated regulation of the NFKB and TP53 pathways. *Autophagy* **2016**, *12*, 999−1014.
(45) Nishanth, R. P.; Jyotsna, R. G.; Schlager, J. J.; Hussain, S. M.; Reddanna, P. Inflammatory responses of RAW 264.7 macrophages upon exposure to nanoparticles: Role of ROS-NFκB signaling pathway. *Nanotoxicology* **2011**, *5*, 502−516.
(46) Liu, L.-J.; Wang, W.; Huang, S.-Y.; Hong, Y.; Li, G.; Lin, S.; Tian, J.; Cai, Z.; Wang, H.-M. D.; Ma, D.-L.; Leung, C.-H. Inhibition of the Ras/Raf interaction and repression of renal cancer xenografts in vivo by an enantiomeric iridium(iii) metal-based compound. *Chem. Sci.* **2017**, *8*, 4756−4763.
(47) Tan, C.; Lai, S.; Wu, S.; Hu, S.; Zhou, L.; Chen, Y.; Wang, M.; Zhu, Y.; Lian, W.; Peng, W.; Ji, L.; Xu, A. Nuclear Permeable Ruthenium(II) β-Carboline Complexes Induce Autophagy To Antagonize Mitochondrial-Mediated Apoptosis. *J. Med. Chem.* **2010**, *53*, 7613−7624.

DOI: 10.1021/acs.inorgchem.9b03006
Inorg. Chem. XXXX, XXX, XXX−XXX